JOURNAL OF SPACECRAFT AND ROCKETS
Vol. 42, No. 4, July–August 2005

Number of Arcs Estimated on Solar Array of a Geostationary Satellite

Mengu Cho*
Kyushu Institute of Technology, Kitakyushu 804-8550, Japan
Shirou Kawakita,† Masao Nakamura,‡ Masato Takahashi,§ and Tetsuo Sato§
Japan Aerospace Exploration Agency, Ibaraki 305-8505, Japan
and
Yukishige Nozaki¶
NEC Toshiba Space Systems, Ltd., Yokohama 224-8555, Japan

Plasma parameters of geosynchronous orbit measured by Los Alamos National Laboratory satellites are analyzed statistically. For each set of plasma parameters, charging analysis is carried out, taking a geostationary satellite representing a typical telecommunication satellite as an example. The number of expected trigger arcs on a solar array is calculated based on the charging duration with severe inverted potential gradient conditions expected in orbit. Using the number of trigger arcs, an appropriate duration of electrostatic discharge ground test is proposed to test the insulation strength against sustained arc phenomena.

Nomenclature

C_{ext}	=	external capacitance, F
I_{sc}	=	solar array short circuit current, A
N_c	=	number of cells per string of a test coupon
N_{cr}	=	critical arc number
N_{exp}	=	number of arcs expected at positive end of solar array string circuit
n_e	=	electron density, cm^{-3}
n_i	=	ion density, cm^{-3}
n_{iH}	=	high-energy ion density, cm^{-3}
T_e	=	electron temperature, keV
T_i	=	ion temperature, keV
T_{iH}	=	high-energy ion temperature, keV
T_{iL}	=	low-energy ion temperature, keV
t	=	charging time, s
t_{esd}	=	time to reach $\Delta V = 400$ V, s
V_b	=	bias voltage, V
V_{cell}	=	cell voltage, V
V_{out}	=	solar array output voltage, V
ΔV	=	differential voltage, V
ϕ_{cg}	=	coverglass potential, V
ϕ_{sat}	=	satellite potential, V

Introduction

SINCE the previous decade, the power level of geostationary satellites has increased dramatically to nearly 10 kW or even higher. To manage the large amount of power efficiently, nowadays many commercial telecommunication satellites employ a solar array that generates electricity at 100 V.

As the voltage of a solar array increases to 100 V, arcing during substorms has been recognized as a serious hazard that sometimes threatens the stable supply of solar array power. In geosynchronous orbit (GEO), when a satellite receives sunlight, its charging is dominated by photoelectrons. As long as the satellite surface is well illuminated under the quiet (nonsubstorm) condition, photoelectrons keep the satellite potential within a few electron volts from the plasma potential. An insulator surface such as a coverglass has similar potential. When a satellite encounters a substorm, however, the current due to high-energy electrons increases and sometimes exceeds the current due to photoelectrons. Then the potentials of the satellite body and the insulator surface can become negative. Due to difference in secondary electron emission coefficients, the insulator potential may drop slower than that of the satellite body. During that process, the coverglass potential can be more positive than that of the nearby conductor (e.g., the interconnector). This situation is called "inverted potential gradient." In the present paper we refer to the potential difference between the coverglass and the satellite body as differential voltage. The differential voltage ΔV is defined in the following equation:

$$\Delta V = \phi_{\text{cg}} - \phi_{\text{sat}} \tag{1}$$

where the satellite potential is equal to the interconnector potential at the negative end of the solar array circuit. As the differential voltage builds up between coverglass and interconnector, an arc may occur. It is well known that an arc occurs once the differential voltage reaches 100 or 200 V under low-Earth-orbit (LEO) plasma condition.[1,2] Cho et al.[3] found that an arc may occur with differential voltage of as low as 400 V under simulated GEO plasma conditions during a ground experiment.

If an arc occurs as a single pulse, it is called a trigger arc or a primary electrostatic discharge (ESD). The risk of one trigger arc growing to a catastrophic arc by receiving energy from the solar array has increased recently as the power level of solar arrays has increased. When an arc occurs, arc plasma may short-circuit two points on the solar array panel with different potentials if certain conditions are met. The solar array string circuit can provide energy to the arc plasma and the short-circuit current keeps flowing until a permanent conductive path is formed between the two points. Once a trigger arc grows to this level, it is called a "sustained arc." The two points can be cells on the same string (intrastring sustained arc), cells on different strings (interstring sustained arc), or a cell and conductive aluminum honeycomb substrate (string–substrate sustained arc). Several satellites[4,5] lost a part of their solar array output power because of a sustained arc. The risk of sustained arc occurrence increases as the voltage of a solar array increases, because the potential

Received 25 November 2003; revision received 23 May 2004; accepted for publication 2 June 2004.

*Associate Professor, Department of Electrical Engineering; cho@ele.kyutech.ac.jp. Senior Member AIAA.
†Engineer, Institute of Space Technology and Aeronautics.
‡Scientist, Institute of Space Technology and Aeronautics.
§Associate Senior Engineer, Office of Space Applications.
¶Assistant Manager, Space Systems Department.

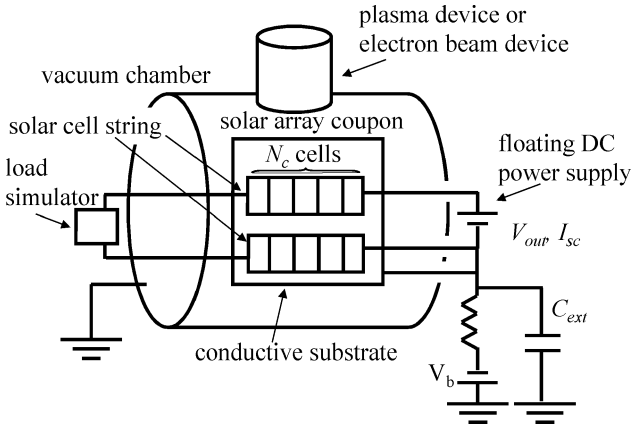

Fig. 1 Experimental layout of a typical ESD ground test with a solar array coupon.

difference between the two points short-circuited by the arc plasma becomes higher.

As size and price of GEO satellites become larger, there is a greater demand for careful ground tests before launch. Ground tests are carried out to confirm whether a given solar array design can withstand the sustained arc. In Fig. 1 we schematically illustrate the experimental layout of a typical ground test. We place a solar array coupon inside a vacuum chamber. The coverglass surface is charged more positively than the solar cells, either by an energetic electron beam or by positive ions. One string of solar cells is biased to a positive potential with respect to the conductive substrate, simulating the positive end of a solar array. Another string is grounded (or sometimes connected through a resistance) to the conductive substrate, simulating the negative end of a solar array. The positive potential given to the first string should be equivalent to the solar array output voltage V_{out}. The floating power supply simulates the solar array string circuit. The power supply should give a constant voltage between the strings before an arc and should give a constant current once the arc plasma short-circuits the strings or the string and the substrate. The maximum current provided by the power supply should be equivalent to the solar array short-circuit current I_{sc}.

When we carry out an ESD test, proper test conditions that simulate the conditions in orbit are necessary. Inadequate testing conditions lead to unexpected failure in space. Increasing the level of harshness beyond a reasonable limit is not always a good solution. There is not yet any standard for performing the ESD test on a solar array. Because manufacturers, subcontractors, launchers, users, and insurers of GEO telecommunication satellites have become international, there is a greater need of an international standard for the ESD test method.

There are currently four major issues regarding the ESD test method:

1) How do we charge the coverglass to produce the inverted potential gradient?

2) What type of power supply do we use to simulate the solar array string circuit?

3) How do we implement the role of capacitance represented by the coverglass of a solar array panel that cannot be accommodated into the vacuum chamber?

4) How long do we carry out the test?

The purpose of the present paper is to answer the last question.

In the present paper, we calculate the number of trigger arcs expected to occur during the operational lifetime. To do so, we must first calculate the total duration of the inverted potential gradient. The number of trigger arcs is derived with assumptions about the arc rate. To calculate how often the inverted potential gradient occurs, we first carry out statistical analysis of the GEO plasma environment. We use data of the Los Alamos National Laboratory (LANL) satellites available from the Coordinated Data Analysis Web (CDAWeb).[6] We identify combinations of plasma parameters, such as, n_e, n_i, T_e, and T_i, that can occur in GEO. Once the combinations are identified, we run the NASCAP/GEO[7] simulation for all the combinations of plasma parameters at each local time. We calculate the total duration for when the differential voltage exceeds a certain threshold value. Because we know the duration of the inverted potential gradient, we can derive the number of arcs by dividing the duration by time for the differential voltages to reach the threshold.

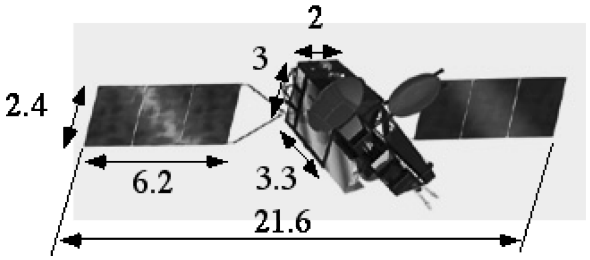

Fig. 2 Schematic picture of WINDS; sizes are shown in meters.

As an example of a GEO satellite, we use the Wideband Internetworking Engineering and Demonstration Satellite (WINDS), which will be launched in 2005 by the Japan Aerospace Exploration Agency. A schematic picture of WINDS is shown in Fig. 2. The satellite has 8760 triple-junction solar cells that generate 5.2 kW of power at 50 V bus voltage. We chose WINDS because of the following three reasons: 1) the satellite properties, especially the surface materials, are known in detail; 2) the satellite has the generic shape of a conventional three-axis stabilized GEO telecommunication satellites; and 3) an ESD test was planned and we had to determine the test duration.

In the second part of this paper, we describe the statistical data of the GEO plasma environment. In the third part, we describe the NASCAP simulation. In the fourth part we present the numerical results derived from the two analyses. In the fifth part, we discuss the uncertainty of the results. In the sixth part, we propose an appropriate ground-test duration. In the last part, we conclude the paper with suggestions for future work.

Statistical Analysis of GEO Plasma Environment

We used data from five LANL satellites: LANL 1989-046, 1991-080, 1990-095, 1994-084, and 97A. At the CDAWeb site, magnetospheric plasma analyzer (MPA)[8] data are listed for n_e, T_e, n_{iH}, n_{iL}, T_{iH}, and ϕ_{sat} at approximately every 90 s. The low energy denoted by the subscript L indicates energy between 1 and 130 eV. The high energy denoted by the subscript H indicates energy between 130 eV and 45 keV. The energy range for electrons is between 30 eV and 45 keV. MPA data give two temperatures: perpendicular and parallel to the geomagnetic field. Because the difference is insignificant for the present purpose, we use the parallel temperature for the statistical analysis.

Although we usually run the NASCAP simulation by assuming a double Maxwellian distribution function for electrons and ions, we can still run it even with a single Maxwellian. During a severe charging case where the satellite potential drops to a large negative value, the low-energy ions are observed to behave like the high-energy ions as they are accelerated. Therefore, we neglect the low-energy ion density n_{iL} and simplify the GEO plasma condition by using a single Maxwellian defined by the parallel temperature.

We downloaded 7.5×10^6 data points from CDAWeb. The data span the period from 15 March 1993 to 24 September 2003. Because one data point corresponds to 90 s in orbit, 7.5×10^6 data points are equivalent to 21 years in orbit. Because all five satellites lacked data from time to time, the total number of data points is not equivalent to that for a 50-year time period in orbit.

We first divide the data into nine zones of local time. The first zone is the eclipse, denoted LT0e in this paper. The other zones each have a duration of 3 h. The second local time zone is from 2230 to 0130 hrs under the sunlit condition denoted as LT0n. The third one is from 0130 to 0430 hrs, denoted as LT3, and so on. We consider a distribution function in a four-dimensional space that consists of the four parameters n_e, n_i, T_e, and T_i. We define 556 four-dimensional

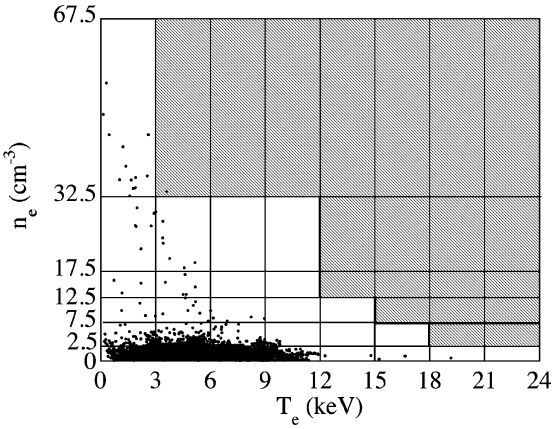

Fig. 3 Example of data of plasma parameters observed between LT4:30 and LT7:30 on LANL 1990.

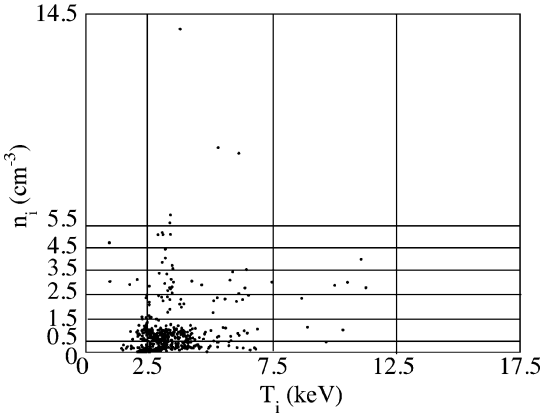

Fig. 4 Ion density and temperature of data points plotted inside a block defined by $2.5 < n_e$ 7.5 cm^{-3} and $3 < T_e$ 6 keV.

volumes that categorize the combinations of n_e, n_i, T_e, and T_i and calculate the probability that a satellite encounters the plasma condition inside a given four-dimensional volume. The maximum values accounted for each parameter are 70 cm^{-3}, 100 cm^{-3}, 24 keV, and 17.5 keV for n_e, n_i, T_e, and T_i, respectively. The four-dimensional volumes are not equally spaced. In Fig. 3, we show an example of how we categorize n_e and T_e. The figure plots a fraction of data between 0430 and 0730 hrs (i.e., LT6 of LANL 1990). We divide the combination of n_e and T_e into rectangular blocks shown in Fig. 3. Each block is further divided into subblocks made of n_i and T_i. In Fig. 4, we show the subblocks inside the block defined by $2.5 < n_e \leq 7.5$ cm^{-3} and $3 < T_e \leq 6$ keV shown in Fig. 3. Each subblock corresponds to one of the four-dimensional volumes. We count the number of data points within each four-dimensional volume. By dividing the number of data points by the total number of data points within a given local time zone, we obtain the probability that a combination of plasma parameters lies in each four-dimensional volume. In the NASCAP simulation, we use the center value of each four-dimensional volume as input parameters.

In Table 1, we list the ranges of parameters used to divide them into the four-dimensional volumes and the center value of each. If we divide n_e, T_e, n_i, and T_i into six, eight, seven, and four cases and consider all the possible combinations of each case, the total number of four-dimensional volumes is $6 \times 8 \times 7 \times 4 = 1344$. Each NASCAP simulation takes approximately 10 min. To reduce the computational time, we neglect the four-dimensional volumes where very few data points exist. The larger the parameter values, the fewer data exist. In Fig. 5 we show the parameter matrix considered for the NASCAP simulation. In the matrix, the shaded blocks are ignored. In each block made of n_e and T_e, we list the number of combinations considered for the values of n_i and T_i. For example, "2×4" means

Table 1 Range of each parameter used to divide the combinations into four-dimensional volumes

	n_e, cm^{-3}		T_e, keV		n_i, cm^{-3}		T_i, keV	
Index	Range	N[a]	Range	N	Range	N	Range	N
1	0–2.5	1.25	0–3	1.5	0∼0.5	0.25	0∼2.5	1.25
2	2.5–7.5	5	3–6	4.5	0.5∼1.5	1	2.5∼7.5	5
3	7.5–12.5	10	6–9	7.5	1.5∼2.5	2	7.5∼12.5	10
4	12.5–17.5	15	9–12	10.5	2.5∼35	3	12.5∼17.5	15
5	17.5–32.5	25	12–15	13.5	3.5∼4.5	4		
6	32.5–67.5	50	15–18	16.5	4.5∼5.5	5		
7			18–21	20.5	5.5∼14.5	10		
8			21–24	22.5				

[a]The columns denoted by N list the values used as the input parameter of the NASCAP simulation.

Table 2 Additional 52 combinations of the parameters used for the statistical data analysis (The values used as input parameters of the NASCAP simulation are listed.)

n_e, cm^{-3}	T_e, keV	n_i, cm^{-3}	T_i, keV
5	1	17.25, 30, 50, 70, 90	1, 6
15	1	17.25, 30	1, 6
25	1	17.25, 30, 50	1, 6
35	1	17.25, 30, 50, 70	1, 6
45	1	17.25, 30, 50.70, 90	1, 6
55	1	17.25, 30, 50, 70, 90	1, 6
65	1	70, 90	1, 6

		T_e, keV							
		1.5	4.5	7.5	10.5	13.5	16.5	19.5	22.5
n_e cm^{-3}	1.25	7x4	7x4	7x4	7x4	7x4	7x4	7x4	7x4
	5	7x4	6x4	6x4	6x4	6x4	6x4		
	10	7x4	2x4	2x4	2x4	2x4			
	15	7x4	2x4	2x4	2x4				
	25	1x4	1x4	1x4	1x4				
	50	1x4							

Fig. 5 Parameter matrix considered for the NASCAP simulation. The shaded blocks are ignored. In each block made of n_e and T_e, the number of combinations considered for the values of n_i and T_i are shown.

that we consider the combinations of the first two values of n_i (0.25 and 1 cm^{-3}) and the four values of T_i (1.25, 5, 10, and 15 keV). In this way, we can reduce the total number of combinations to 504, which covers 99.8% of all the data points. To improve the coverage, we add extra combinations where extremely high electron and ion densities are observed. In Table 2, we list the additional combinations of the parameters, and we list only the input parameters used for the NASCAP simulation. The data range for n_e is every 10 cm^{-3} from 0 to 70 cm^{-3}. The range for T_e is from 0 to 2 keV. The data range for n_i is $14.5 < n_i$ 20 cm^{-3} and every 20 cm^{-3} from 20 to 100 cm^{-3}. The data range for T_i is $0 < T_i$ 2 keV and $2 < T_i$ 10 keV. The values in Table 2 correspond to the center values of each four-dimensional volume. Including the additional 52 combinations, the total of 556 four-dimensional volumes covers 99.978% of all the data points.

NASCAP Simulation

Figure 6 shows the NASCAP/GEO model of WINDS. The satellite surface is modeled as black Kapton® and indium tin oxide (ITO) on an optical surface reflector (OSR). One side of the solar array panel is coverglass and the other side is carbon-fiber-reinforced plastic (CFRP). The material properties used for the NASCAP simulation are listed in Table 3. For simplicity, we neglected radiation-induced conductivity in the simulation. Properties 9 and 10 for coverglass, ITO, and CFRP are not as listed as in Table 3. They are, in fact, the material density in grams per cubic centimeter and mean molecular weight in atomic mass units, respectively. They are used

Table 3 Material properties of WINDS assumed for the NASAP simulation (see text for parameters 9 and 10 of coverglass, ITO, and CFRP)

No.	Property	Unit	Black Kapton	Cover glass	ITO + OSR	CFRP
1	Relative dielectric constant	None	3.50E+00	6.99E+00	1.00E+00	4.30E+00
2	Dielectric material thickness	m	2.54E−05	1.00E−04	1.00E−06	2.00E−04
3	Bulk conductivity (−1 for a metallic conductor)	1/*m	−1.00E+00	1.0E−12/1.0E−16	−1.00E+00	−1.00E+00
4	Atomic number	None	4.50E+00	2.00E+01	2.44E+01	5.00E+00
5	Maximum secondary electron yield for electron impact	None	9.30E−01	1.10E+01	1.40E+00	2.10E+00
6	Primary electron energy that produces maximum secondary yield	keV	2.80E−01	8.00E−01	8.00E−01	1.50E−01
7	Range parameters R = P7Ep8 + P9ep10	Å	1.80E+02	−1.00E+00	−1.00E+00	−1.00E+00
8	Range parameters R = P7Ep8 + P9ep10	None	4.50E−01	0.00E+00	0.00E+00	0.00E+00
9	Range parameters R = P7Ep8 + P9ep10	Å	3.12E+02	2.50E+00*	7.30E+00*	1.70E+00*
10	Range parameters R = P7Ep8 + P9ep10	None	1.75E+00	2.03E+01*	5.55E+01*	1.77E+00*
11	Secondary electron yield due to impact of 1 keV protons	None	4.55E−01	4.55E−01	4.90E−01	4.55E−01
12	Incident proton energy that produces maximum secondary electron yield	keV	8.00E+01	1.40E+02	1.23E+02	1.40E+02
13	Photoelectron yield for normally incident sunlight	A/m^2	7.20E−06	1.50E−05	1.50E−05	4.00E−06
14	Surface resistivity (−1 for nonconducting surface)	/m^2	−1.00E+00	2.50E+16	−1.00E+00	−1.00E+00
15	Maximum (absolute) potential attainable before a discharge must occur	volts	1.00E+04	2.75E+04	1.00E+04	1.00E+04
16	Maximum potential difference between surface and underlying conductor before a discharge must occur	volts	2.00E+03	2.00E+03	2.00E+03	2.00E+03

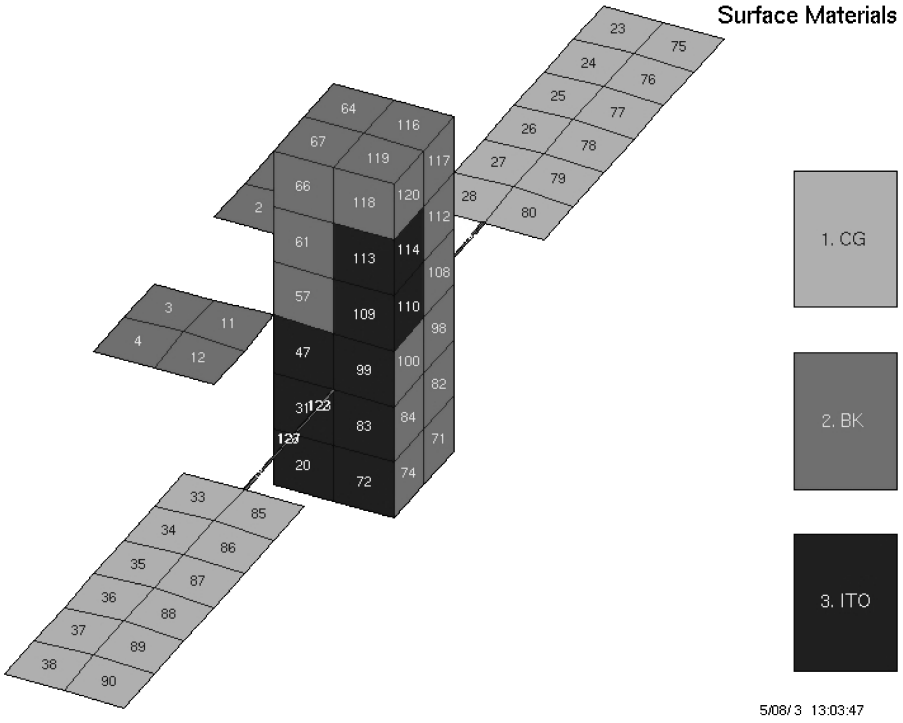

Fig. 6 NASCAP simulation model of WINDS.

to calculate the range of electrons in each material based on the approximation formula given by Feldman.[9] The NASCAP/GEO code is not designed to run by an automatic script. Each case must be run manually. To run more than 2000 cases, we developed a script program written in Perl that enables us to launch the simulation code automatically with different input parameters.

Tables 1 and 2 list the values used as the input parameters for the plasma conditions. The plasma is modeled as a single Maxwellian. For each combination of plasma parameters described, we consider the cases where the local time of the satellite is 0000 hrs in eclipse, 0000 hrs in noneclipse, 0600 hrs, 1200 hrs, and 1800 hrs. When the local time is any of 0300, 0900, 1500, or 2100 hrs, the satellite receives oblique solar illumination. Because it is very difficult to model the oblique solar incidence on a rectangular satellite via NASCAP/GEO, we do not run the NASCAP simulations for those four local time zones; we interpolate the results of adjacent local time zones.

In the NASCAP simulation, we mainly look at coverglass potential. Figure 7 shows how the NASCAP simulation converges to a steady-state potential. In the figure, we plot the satellite potential and the potential of the coverglass located at the far end of the solar array paddle. The satellite potential and the coverglass potential drop to negative values with different time scales. In this example, both the satellite and the coverglass are illuminated by the sunlight and the differences of secondary electron current and photoelectron current are the causes of the different time scales. A similar result was presented by Katz et al.[4] to explain the anomaly on the TEMPO-2 satellite. With different sets of parameters, the potentials show different temporal variations. For some cases, the potentials show oscillation before they reach steady-state values.

The purpose of the NASCAP simulation is to identify the sets of plasma parameters that produce the inverted potential gradient. Therefore, we stop each run of the NASCAP simulation if we determine that no significant differential voltage will build up. The criteria

Table 4 Sets of plasma parameters with the probability of occurrence higher than 1%; the differential voltages of the coverglass at the far end of the solar array paddle calculated by the NASCAP simulation are also listed

Plasma parameters				Probability of occurrence									NASCAP result ΔV				
T_e, keV	n_e, cm^{-3}	T_i, keV	n_i, cm^{-3}	LT0e, %	LT0n, %	LT3, %	LT6, %	LT9, %	LT12, %	LT15, %	LT18, %	LT21, %	LT0e, V	LT0n, V	LT6, V	LT12, V	LT18, V
1.5	1.25	1	0.25	0	2	2	5	6	2	0	0	2	10	3	6	3	3
1.5	1.25	1	1	0	0	2	4	2	1	0	0	0	8	8	6	8	8
1.5	1.25	5	1	46	48	57	56	49	39	36	40	44	2	5	3	7	5
1.5	1.25	5	0.25	6	8	14	24	34	39	28	19	12	6	3	6	3	3
1.5	1.25	5	2	3	2	1	1	0	0	0	1	1	4	6	5	6	6
1.5	1.25	10	1	11	19	7	2	1	8	23	32	30	5	5	8	7	7
1.5	1.25	10	0.25	1	2	1	0	0	6	8	3	3	7	3	4	3	3
1.5	1.25	10	2	0	0	0	0	0	0	0	0	1	2	7	7	7	7
4.5	1.25	5	1	8	3	5	1	0	0	0	0	0	1517	5	6	7	4
4.5	1.25	5	2	1	0	0	0	0	0	0	0	0	708	8	5	9	8
4.5	1.25	10	1	10	4	2	0	0	0	0	0	0	1108	7	7	5	6
4.5	1.25	10	0.25	2	1	0	0	0	0	0	0	0	3106	2	2	5	3

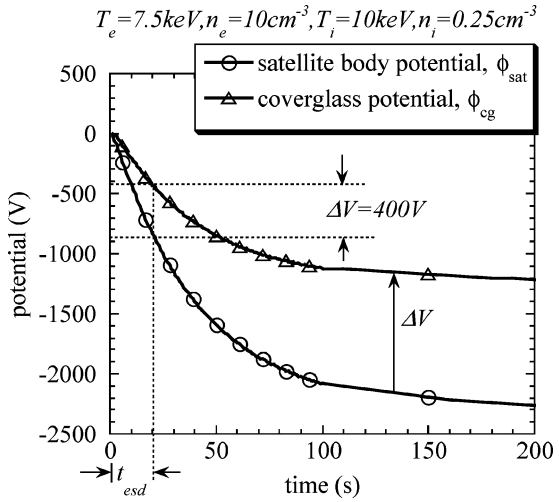

Fig. 7 Example of temporal variations of the potentials calculated by the NASCAP simulation. The potentials of the satellite body and the coverglass at the far end of the solar array paddle are shown. The definitions of ΔV and t_{esd} are also shown.

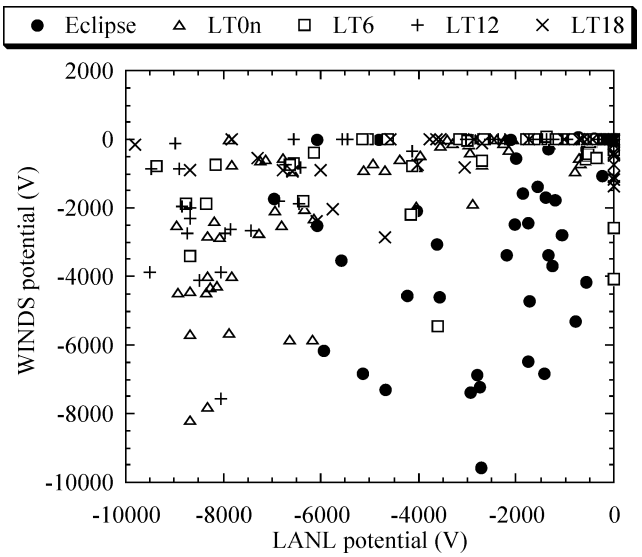

Fig. 8 Relationship between the WINDS body potential calculated by the NASCAP simulation and the average of the LANL satellite body potential observed for the same set of plasma parameters.

we use are the satellite potentials: $\phi_{sat} > 0$ at $t = 10$ s, $\phi_{sat} > -10$ V at $t = 100$ s, or $\phi_{sat} > -100$ V at $t = 100$ s, where the time t is counted from the beginning of the simulation. Even if the satellite potential shows a significant negative potential, we stop the simulation at $t = 5000$ s.

In the NASCAP model shown in Fig. 6, each solar array paddle is divided into 12 segments. We look at the coverglass potential at the far end of the paddle, because that is the point where the maximum differential voltage appears. We calculate the time for the differential voltage at that point to reach 400 V. The value of $\Delta V = 400$ V is chosen from the threshold for arc inception.[3] We define the arc interval t_{esd} by the time to reach $\Delta V = 400$ V. The definition is also shown in Fig. 7. We may assume that, once the differential voltage of 400 V is built up, an arc occurs somewhere on the solar array paddle.

Numerical Results

In Fig. 8 we plot the WINDS potential calculated by the NASCAP simulation for each case of the plasma parameters and the average of satellite potential observed by LANL satellites. This calculation has been made to check whether the NASCAP simulation gives reasonable results. During eclipse, WINDS charges more negatively than LANL satellites. On the other hand, during sunlit conditions, WINDS charges less negatively. This can be explained if WINDS has more exposed conductive area illuminated by the sunlight than LANL satellites. Ideally, to check numerical accuracy, the NASCAP simulation should be run with the parameters of the LANL satellites. Unfortunately, the parameters of the LANL satellites, including size, shape, and material properties, are unknown. Although quantitative accuracy must be checked with another method, Fig. 8 is still sufficient to say that the NASCAP simulation produces qualitatively reasonable outputs.

Table 4 lists the sets of plasma parameters with a probability higher than 1% at each local time zone. During the eclipse, as electron temperature increases to 4.5 keV, the differential voltage can exceed 1000 V. From Table 4, during the eclipse the differential voltage exceeds 1000 V with a probability higher than 20%. As the satellite is illuminated by the sunlight, however, photoelectrons maintain the satellite potential and the differential voltage does not develop easily. For all the cases listed in Table 4, none of the noneclipse cases shows $\Delta V > 10$ V. Therefore, during the daytime, inverted potential gradient with a large ΔV occurs only as an exceptional case.

Table 5 lists the case where the NASCAP simulation result gives $\Delta V > 400$ V and the probability of occurrence in any local time zone is higher than 0.01% under the sunlit condition. The combination of high electron temperature (4.5 keV), high electron density (5 cm^{-3}), and low ion density (0.25 cm^{-3}) provides such conditions. The ion temperature T_i has a relatively small influence on the differential voltage. It is quite reasonable that the increased electron flux lowers the satellite potential and the difference of currents due to secondary electrons and photoelectrons results in the large

differential voltage. Although the 13 cases in Table 5 give severe charging, this type of occurrence is limited. The highest probability of occurrence is 0.081% for the bottom row (i.e., $T_e = 4.5$ keV, $n_e = 5$ cm^{-3}, $T_i = 10$ keV, $n_i = 0.25$ cm^{-3}) at LT12.

By summing the probabilities of all the cases showing $\Delta V > 400$ V at each local time zone, and multiplying the sum by $8760 (= 365 \times 24)$ h, we obtain the total charging duration when the differential voltage exceeds 400 V in one year. Table 6 lists the total charging duration. In the table, the values of LT3, LT9, LT15, and LT21 have been interpolated from the adjacent time zones and the sunlit total denotes the sum of the charging duration, excluding LT0e. From this table, it is concluded that the satellite suffers severe charging with $\Delta V > 400$ V for approximately 12 h/year while the solar array generates electricity. If position and scale of a trigger arc meet certain conditions, there is a risk that the trigger arc will become a sustained arc because the solar array can provide DC power into the arc plasma. In Table 6 we also list the numbers derived by varying the criteria of the differential voltage ΔV. Even if we set optimistic criteria, such as $\Delta V > 1000$ V, the satellite still goes through the severe charging situation for 6.5 h in one year. Lowering the criteria to 300 V increases the total charging time to 14 h/year.

In Table 6, the charging duration at LT12 is longer than that at LT6 for $\Delta V > 400$ V. It is usually considered that surface charging is most severe in the early morning because energetic electrons accelerated from the geomagnetic tail impact on a satellite as they drift due to the horizontal electric field.[2] In Fig. 9 we plot the probability of occurrence of $n_e > 10$ cm^{-3} and $T_e > 3$ keV at each local time measured by the LANL satellites. Indeed, there are more likely to be energetic electrons in the early morning but the extremely dense electrons are often observed between the local noon and late morning. Although this observation is very interesting, an explanation is beyond the scope of the present paper. The high number of charging duration at LT12 listed in Table 6 is due to the events of extremely dense electrons.

Once we identify the cases where the differential voltage exceeds 400 V, we can also estimate the total number of arcs expected in orbit. Because the time for the differential voltage to reach 400 V, t_{esd}, can be regarded as the time interval of a series of repeated trigger arcs, we can calculate the number of arcs by dividing the expected duration of cases having $\Delta V > 400$ V as listed in Table 5 by t_{esd}. Table 7 lists the expected number of arcs for each case listed in Table 5.

By taking the sum of the expected numbers of arcs of all the cases, including the cases not listed in Table 7, we obtain the total number of arcs expected in one year. For the local time zones, LT3, LT9, LT15, and LT21, we interpolate the numbers of adjacent time zones. After all, the total number of arcs expected in one year is 2990, among which 556 are expected during the eclipse and 2434 are expected during the sunlit conditions as listed in Table 8.

The operational life year of WINDS is five years, which is very short for a typical commercial GEO satellite but common for government-sponsored experimental satellites. During the five years, the solar array of WINDS is expected to be under inverted potential gradient with $\Delta V > 400$ V for approximately 60 h while generating electricity. The total number of expected trigger arcs during the five years is 14,950, among which 12,170 arcs will occur during the power generation. Although more than 10,000 trigger arcs sounds enormous, we expect only a few arcs per cell if we consider the fact that a large GEO satellite carries nearly 10,000 solar cells. WINDS has 8760 cells and each solar cell is expected to suffer only one or two arcs on average.

Uncertainty Analysis

We should mention the uncertainty of the numerical results presented in this paper. Several factors cause the uncertainty, such as

Table 5 Sets of plasma parameters with the differential voltage calculated by the NASCAP simulation higher than 400 V and the probability of occurrence higher than 0.01% under the sunlit condition

Plasma parameters				NASCAP result, ΔV				
T_e, keV	n_e, cm^{-3}	T_i, keV	n_i, cm^{-3}	LT0e, V	LT0n, V	LT6, V	LT12, V	LT18, V
13.5	5	5	0.25	16,890	2244	2142	2198	2251
10.5	10	10	0.25	16,440	2931	2836	2884	2940
10.5	5	10	0.25	13,840	1716	1628	1680	1725
10.5	5	5	0.25	13,280	1723	1636	1685	1731
7.5	10	10	0.25	11,630	2012	1935	1976	2017
7.5	10	5	0.25	11,240	2015	1942	1987	2022
7.5	5	10	0.25	9,760	1133	1056	1109	1136
7.5	5	5	0.25	9,480	1141	1064	1117	1145
4.5	10	10	0.25	6,501	925	864	907	928
4.5	10	5	0.25	6,418	931	871	917	934
4.5	5	10	0.25	5,347	419	356	410	421
4.5	5	5	0.25	5,336	429	365	419	430
4.5	5	1.25	0.25	4,850	437	373	427	438

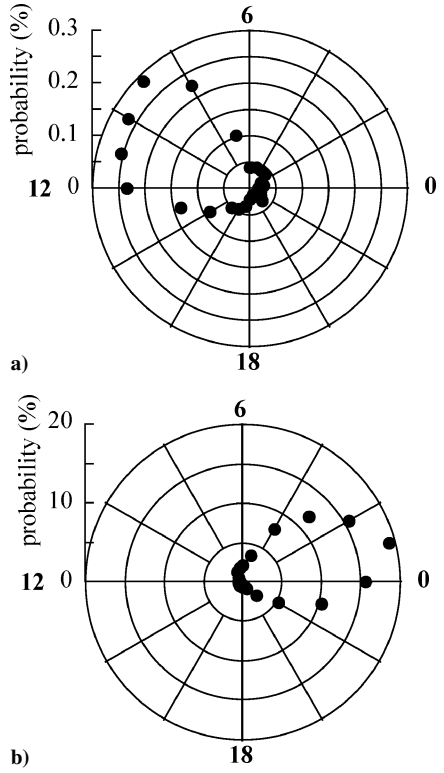

Fig. 9 Probability of occurrence for a) $n_e > 10$ cm^{-3} and b) $T_e > 3$ keV observed on LANL satellites at each local time. The data during the eclipse are not included.

Table 6 Total charging duration expected in one year when the differential voltage exceeds a value listed in the first column

Criteria of charging	Charging duration, h/yr									Sunlit total, h/yr
	LT0e	LT0n	LT3	LT6	LT9	LT12	LT15	LT18	LT21	
300	22.28	0.89	(1.77)	2.58	(2.68)	2.79	(1.74)	0.68	(0.83)	13.96
400	22.28	0.78	(1.26)	1.68	(2.20)	2.71	(1.69)	0.66	(0.75)	11.72
600	22.28	0.47	(1.09)	1.68	(1.58)	1.48	(0.89)	0.30	(0.40)	7.88
800	20.81	0.45	(1.08)	1.68	(1.57)	1.47	(0.87)	0.28	(0.38)	7.79
1000	20.79	0.33	(0.89)	1.41	(1.33)	1.24	(0.74)	0.23	(0.30)	6.47

Table 7 Expected number of trigger arcs for cases listed in Table 5

Plasma parameters				Duration in one year, s					Time to reach $\Delta V = 400$ V, s					Number of arcs in one year				
T_e, keV	n_e, cm^{-3}	T_i, keV	n_i, cm^{-3}	LT0e	LT0n	LT6	LT12	LT18	LT0e	LT0n	LT6	LT12	LT18	LT0e	LT0n	LT6	LT12	LT18
13.5	5	5	0.25	0	290	106	439	33	8	9	10	9	9	0	32	11	49	4
10.5	10	10	0.25	0	0	448	156	29	5	6	6	6	6	0	0	75	26	5
10.5	5	10	0.25	4	55	558	507	194	9	12	12	12	12	0	5	47	42	16
10.5	5	5	0.25	0	154	321	405	70	9	12	12	12	12	0	13	27	34	6
7.5	10	10	0.25	4	13	220	329	70	7	8	8	8	8	1	2	28	41	9
7.5	10	5	0.25	0	34	313	173	83	7	8	8	8	8	0	4	39	22	10
7.5	5	10	0.25	8	111	1848	925	112	13	18	20	19	18	1	6	92	49	6
7.5	5	5	0.25	4	145	773	650	157	13	18	20	19	18	0	8	39	34	9
4.5	10	10	0.25	0	38	525	215	21	13	20	22	21	20	0	2	24	10	1
4.5	10	5	0.25	0	90	399	177	103	13	20	22	21	20	0	5	18	8	5
4.5	5	10	0.25	0	175	0	3184	673	26	140	N/A	170	140	0	1	0	19	5
4.5	5	5	0.25	4	249	0	887	549	26	120	N/A	140	120	0	2	0	6	5
4.5	5	1.25	0.25	0	148	0	0	0	26	110	N/A	130	110	0	1	0	0	0

Table 8 Total number of trigger arcs in one year expected at each local time zone

Local time zone	Number of trigger arcs
LT0e	556
LT0n	151
LT3	(320.5)
LT6	478
LT9	(482.5)
LT12	487
LT15	(291)
LT18	95
LT21	(129)
Total	2990
Sunlit total	2434

Table 9 Charging time and arc rate calculated based on data for each satellite

Satellite	Number of data points	Charging time in the sunlit condition, h/yr	Arcs/yr in the sunlit condition
LANL 1989-046	860,694	26.94	6038
LANL 1990-095	1,212,469	20.57	2974
LANL 1991-080	2,200,727	15.62	3973
LANL 1994-084	2,019,238	3.36	565
LANL 97A	1,275,347	1.81	290
Average		13.66	2768
Standard deviation		10.89	2407
All combined	7,568,475	11.72	2434

variability of the LANL data, uncertainty in the material properties used in the NASCAP simulation, and characteristics of the particular satellite design. To see the effect of variability of the LANL data, in Table 9, we list the total charging time and the number of arcs expected under the sunlit condition in one year that are calculated based on the data of each satellite only. The bottom row of the table lists the numbers calculated based on the data combined from observations of all five satellites, which correspond to the numbers listed in Tables 6 and 8. Although the standard deviation is very large, the averages of the five satellites are close to the numbers calculated by the combined data.

To see the effect of uncertainty of the material properties, we ran an additional case where the standard worst GEO case[10] was assumed to be the plasma condition at 0600 hrs in local time and varied the bulk conductivity of the coverglass. In Fig. 10, we plot the maximum potential difference between the spacecraft body and the coverglass for different values of conductivity. In the NASCAP simulation, we used 1.0×10^{-16} 1/Ω · m for eclipse and 1.0×10^{-12} 1/Ω · m during the sunlit conditions as the default values of the coverglass bulk conductivity. A slight decrease in conductivity would have given many more charging cases. On the other hand, if we had included radiation-induced conductivity, we would have obtained fewer charging cases.

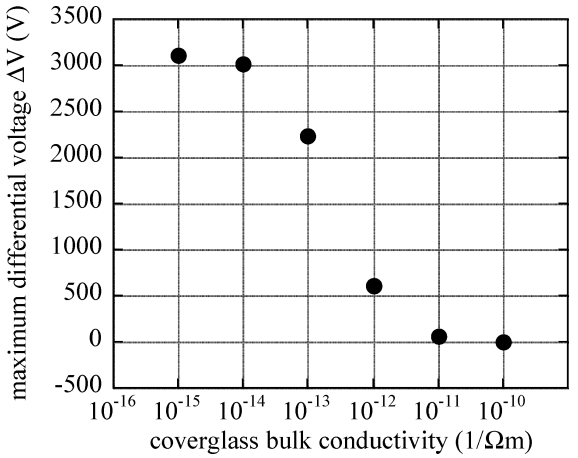

Fig. 10 Maximum differential voltage calculated by NASCAP/GEO for various values of coverglass bulk conductivity under the worst GEO plasma condition at 0600 hrs local time.

To see the effect of particularity of a given satellite design, we calculated the total charging duration for Engineering Test Satellite VIII (ETS8) using the same methodology presented in this paper. Figure 11 shows a schematic picture of ETS8. Its NASCAP/GEO simulation model is discussed in Ref. 11. ETS8 has very large deployable antennas made of gold mesh. Thanks to the very large conductive area exposed to the sunlight, charging of ETS8 is not as severe as that of WINDS. The duration for when the potential difference between the coverglass and the spacecraft body exceeds 400 V is only 6.0 h/year in the sunlit condition, compared to 11.72 h of WINDS.

Discussion

We now come back to the questions raised in the Introduction regarding how long we should carry out the ESD ground test. Two major parameters are relevant to the duration of the ESD test: number of trigger arcs and charging duration in orbit. Generally speaking, to test the insulation strength of a given electrical apparatus, we usually first give an overstress to a test sample and measure the flashover conditions. For the case of the solar array, the purpose of the ESD ground test is to test the insulation strength of the array design against sustained arc, and the flashover corresponds to the sustained arc. Because the flashover is a phenomenon governed by a probability, we usually test many samples to obtain the probability density function that defines the probability of flashover for a given stress (usually the applied voltage). The operational condition of the apparatus is determined by extrapolating the probability density function to calculate the condition where the probability of flashover

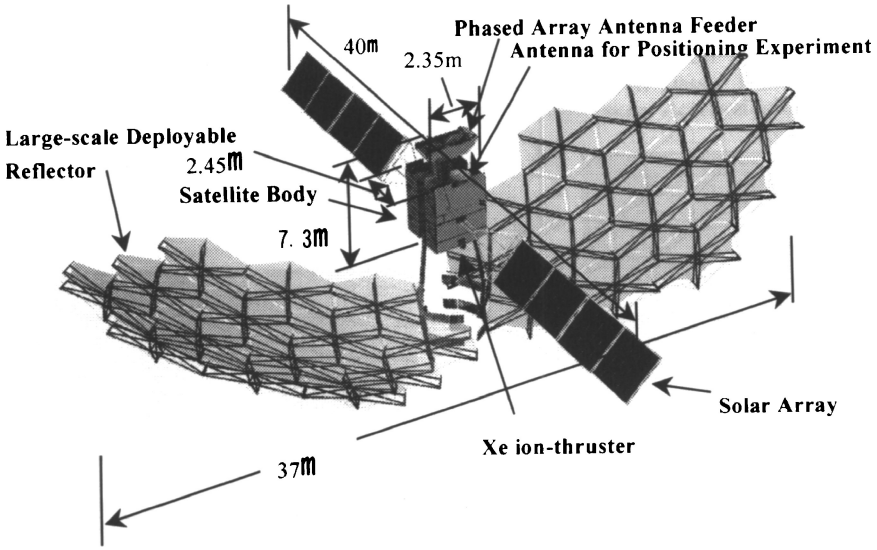

Fig. 11 Schematic picture of ETS8.

is less than an acceptable limit. We also test the apparatus for durability under the operational conditions. If the operational lifetime of the apparatus is very long, we give more severe conditions to accelerate the degradation processes and shorten the test duration.

Typical ESD ground tests differ from the tests mentioned earlier in several points. First, we rarely define the probability function of the sustained arc. To do so, we need to test many test samples and destroy them. Because the tests are carried out in high vacuum, testing many samples requires a significant amount of personnel and facility cost. Second, the degradation mechanism in orbit has not been quantified yet to derive a proper acceleration coefficient for each degradation factor.

Suppose that we count the number of trigger arcs on a given solar cell until the cell suffers sustained arc. Each trigger arc has different characteristics, such as its position, peak current, total energy, and so on, even if it occurs on the same solar cell. If a trigger arc occurs on an interconnector, it is unlikely to become a sustained arc. Even if a trigger arc occurs on a cell edge, the energy associated with the trigger arc might not be enough to have a sustained arc. Finally, a sustained arc occurs as a trigger arc that satisfies all the necessary conditions for the sustained arc formation. If we would measure the number of trigger arcs necessary to have a sustained arc for many cells, the number scatters according to a certain probability density function. One cell may suffer a sustained arc after the first trigger arc. Another may suffer a sustained arc only after thousands of trigger arcs. We can still define the average (or most likely) number of trigger arcs necessary to have a sustained arc. We call this number the critical arc number $N_{\rm cr}$ in the present paper.

The critical arc number is a function of cell parameters such as cell material, distance to adjacent cells, voltage with respect to substrate, voltage across cell gap, current provided by each array string, and so on. Most of the parameters, such as the material, the distance to adjacent cells, or the current of array string, are common to all the cells once the design of the solar array is fixed. Then the critical arc number depends on the position of the solar cell on the array string circuit, which is the cell voltage $V_{\rm cell}$ ranging from 0 to $V_{\rm out}$. Therefore, we have a curve that gives the relationship between $N_{\rm cr}$ and the cell voltage $V_{\rm cell}$, which is shown schematically in Fig. 12. We can easily imagine that $N_{\rm cr}$ decreases as $V_{\rm cell}$ increases because the increased $V_{\rm cell}$ indicates the increased potential difference from the adjacent cells and the conductive substrate.

In a typical ESD ground test using a solar array coupon, we test the situation at the positive end of the solar array string as shown in Fig. 1. At least two strings are mounted on the coupon substrate. One string made of N_c cells is biased positively with respect to the substrate via a floating DC power supply, simulating the positive end of solar array. The test is usually carried out without any significant

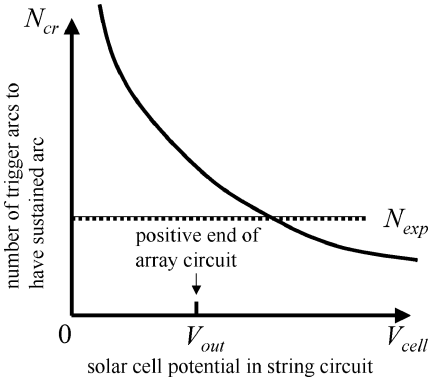

Fig. 12 Schematic picture to explain the relationship between the number of trigger arcs to have sustained arc and the solar cell potential. If the expected number of trigger arcs in orbit, $N_{\rm exp}$, is lower than $N_{\rm cr}$ at $V_{\rm out}$, the sustained arc will not occur in orbit.

light, producing little voltage in the cell. Therefore, the coupon test is equivalent to test N_c samples of the positive end of the array string. The other string is grounded to the substrate, simulating the negative end of the solar array. Because not all of the positive ends of the solar array circuit have the maximum potential difference, $V_{\rm out}$, from the adjacent cells, the layout shown in Fig. 1 corresponds to the most severe case.

We can estimate the number of trigger arcs expected at the positive end of the array string during the satellite lifetime. For the case of WINDS, the total number of trigger arcs in five years is 12,170, considering only the sunlit cases. The WINDS solar array is made of 292 parallel strings. Each string is made of 30 triple-junction solar cells connected in series and the output voltage $V_{\rm out}$ is 55 V. Because the trigger arc in GEO occurs regardless of the cell voltage, the total number of arcs expected for cells with $V_{\rm cell} = V_{\rm out} = 55$ V is $12170/30 = 406$. We denote this number by $N_{\rm exp}$. If we can verify that the sustained arc does not occur even after 406th arc on the N_c cells simulating the positive end of the array, we can say that $N_{\rm exp}$ is less than $N_{\rm cr}$ and the sustained arc will not occur on the cells with $V_{\rm cell} = V_{\rm out}$. Because the expected number of trigger arcs, $N_{\rm exp}$, is the same for other $V_{\rm cell} (< V_{\rm out})$ and $N_{\rm cr}$ increases as $V_{\rm cell}$ decreases, we can safely say that the sustained arc will not occur for other cells on the solar array strings.

We should always recognize, however, the probabilistic nature of arcing. Any two arcs are not exactly the same. Therefore, in a ground test, sufficient margin should be given to $N_{\rm exp}$ to feel more confident that a test with a small-sized coupon can be extrapolated to a

large-sized flight solar panel. In addition to the probabilistic margin, extra margin is necessary to account for the numerical uncertainties of $N_{\exp}$ that are illustrated in the preceding section.

We have identified that WINDS is under the inverted potential gradient for 12 h/year in orbit. Even for a commercial satellite with a 15-year lifetime, the total is $12 \times 15 = 180$ h, which is a manageable number. Through a 180-h (or 60 h for WINDS) ground test, we can test the durability against repeated trigger arcs. Allowing $N_{\exp}$ (typically 100 s or more) trigger arcs on N_c (typically 10 s or less) cells on a test coupon already accelerates the degradation of insulation strength against sustained arc due to repeated trigger arcs because only one or two arcs are expected on a cell in orbit. Therefore, if a test coupon passes the ESD test for the same duration as the total charging duration in orbit (60 h for WINDS), there is no doubt that the solar array design has enough durability. This statement is true, however, only if the degradation of insulation strength against the sustained arc degrades due mostly to repeated trigger arcs and if degradation due to other environmental factors such as UV, thermal cycle, and radiation is insignificant. For many satellites with 100 V bus voltage, the insulation strength is enhanced by grouting an extra amount of room temperature vulcanizing (RTV) silicon adhesive among cells or between a cell and the insulation layer on the substrate. The long-time degradation of RTV due to the environmental factors mentioned earlier is still unknown.

If only the number of trigger arcs is important, we might want to use a dense plasma environment similar to that in LEO to carry out the ESD test, because the arc rate is much higher and we can finish the test quickly. Whether we can use the LEO-like plasma condition to test a solar array for GEO satellites is a point of controversy. To be certain, we need to verify that the sustained arc phenomenon in the LEO-like plasma is similar or at least scalable to the sustained arc phenomenon in the tenuous plasma environment of GEO.

Conclusions

As the power level and voltage of GEO satellites increase, there is greater demand for ESD ground tests on solar arrays. The major purpose of the ESD test is to test the insulation strength of a given solar array design against the destructive sustained arc. The ESD test must be carried out with proper test conditions. To answer the question of how long we should carry out the ESD test, we have calculated the number of trigger arcs expected in orbit.

We have carried out the statistical analysis of the observation data of plasma parameters in GEO using LANL satellite data. For each combination of plasma parameters, a NASCAP simulation series has been carried out to calculate the differential voltage between coverglass and satellite body. We have chosen WINDS as an example of GEO satellites. The solar array will have the inverted potential gradient with the differential voltage higher than 400 V for 12 h in one year in orbit under sunlit conditions. If we assume that the solar array suffers a trigger arc once the differential voltage, ΔV, reaches 400 V, the satellite will suffer 2434 arcs in one year in orbit under sunlit conditions. Because each solar array of the WINDS string consists of 30 cells connected in series, the expected number of trigger arcs at the positive ends of the solar array string is $2434/30 = 81$ in one year.

In conclusion, we propose the following method to determine the appropriate duration of ESD ground tests:

1) For a given satellite, we calculate the expected number of trigger arcs at the positive end during the operational lifetime of the satellite, $N_{\exp}$. To do so, a charging analysis for all the possible combinations of plasma parameters must be made. For the case of WINDS, we have obtained $N_{\exp} = 406$.

2) We produce the inverted potential gradient on a solar array test coupon. The coupon should represent the design-of-flight model and simulate the potential layout at the positive end of the solar array string circuit with the maximum potential difference from the adjacent cells. We let trigger arcs occur on the coupon. If the coupon shows no sustained arc, even after $N_{\exp}$ trigger arcs, we can say that the solar array design has enough insulating strength against the sustained arc. Considering the probabilistic nature of arcing and numerical uncertainty, adding an extra margin to $N_{\exp}$ is recommended.

There seems to be no need to carry out the ESD test longer than the total charging time expected in orbit, namely 60 h for the case of WINDS. Having $N_{\exp}$ trigger arcs on a limited number of solar cells on the test coupon over the same duration as in orbit, however, gives reasonable overstress to each cell. Therefore, it is not a bad practice. We, however, need to know whether the insulation strength degrades due to long-time exposure to UV, thermal cycles, and radiation before we determine the appropriate duration of an ESD test for long-time durability.

Acknowledgments

The authors thank Geoff Reeves of Los Alamos National Laboratory (LANL) and Iku Shinohara of the Institute of Space and Astronautical Science for their help in obtaining data of LANL satellites. The authors also thank Yukako Teshima and Noburo Aoki of the Kyushu Institute of Technology for downloading the data from Coordinated Data Analysis Web and help analyzing the data. Discussion with Kazuhiro Toyoda of Chiba University was also very helpful.

References

[1]Ferguson, D. C., Snyder, D. B., Vayner, B. V., and Galforo, J. T., "Array Arcing in Orbit from LEO to GEO," AIAA Paper 98-1002, Jan. 1998.

[2]Hastings, D. E., and Garrett, H., *Spacecraft-Environmental Interactions*, Cambridge Univ. Press, New York, 1996.

[3]Cho, M., Ramasamy, R., Matsumoto, M., Toyoda, K., Nozaki, Y., and Takahashi, M., "Laboratory Tests on 110V Solar Arrays in a Simulated Geosynchronous Orbit Environment," *Journal of Spacecraft and Rockets*, Vol. 40, No. 2, 2003, pp. 211–220.

[4]Katz, I., Davis, V. A., and Snyder, D. B., "Mechanism for Spacecraft Charging Initiated Destruction of Solar Arrays in GEO," AIAA Paper 98-1002, Jan. 1998.

[5]Bogus, K., Claassens, C., and Lechte, H., "Investigations & Conclusions of the ECS-Solar-Array In-Orbit Power Anomalies," *Proceedings of 18th IEEE Photovoltaic Specialist Conference*, Inst. of Electrical and Electronics Engineers, Piscataway, NJ, Oct. 1985, pp. 368–375.

[6]*Coordinated Data Analysis Web (CDAWeb)*, URL: http://cdaweb.gsfc.nasa.gov/ [cited 1 Dec. 2002].

[7]Rubin, A. G., Katz, I., Mandell, M., Schnuelle, G., Seen, P., Parks, D., Cassidy, J., and Roche, J., "A Three-Dimensional Spacecraft-Charging Computer Code in Space Systems and Their Interactions with Earth's Space Environment," *Space Systems and Their Interactions with Earth's Space Environment*, edited by H. Garret and C. Pike, Vol. 71, Progress in Astronautics and Aeronautics, AIAA, New York, 1980, pp. 318–336.

[8]Bame, S. J., McComas, D. J., Thomsen, M. F., Barraclough, B. L., Elphic, R. C., Glore, J. P., Gosling, J. T., Chaves, J. C., Evans, E. P., and Wymer, F. J., "Magnetospheric Plasma Analyzer for Spacecraft with Constrained Resources," *Review of Scientific Instruments*, Vol. 64, No. 4, 1993, pp. 1026–1033.

[9]Feldman, C., "Range of 1-10 keV Electrons in Solids," *Physical Review*, Vol. 117, No. 2, 1960, pp. 455–459.

[10]Frezet, M., Day, E. J., Granger, J. P., and Hamelin, J., "Assessment of Electrostatic Charging of Satellites in the Geostationary Environment," *ESA Journal*, Vol. 13, No. 2, 1989, pp. 89–116.

[11]Fujii, H., Onodera, N., Murakami, Y., Kawakita, S., Nishimoto, H., and Takahashi, M., "Charging Analysis of Engineering Test Satellite VIII (ETS-VIII) of Japan," *Proceedings of 7th Spacecraft Charging Conference*, ESA, Noordwijk, The Netherlands, 2001, pp. 183–188.

A. Ketsdever
Associate Editor